J Nanostruct 7(4): 273-283, Autumn 2017

RESEARCH PAPER

Dependence of Nanostructure and the Optical Properties of Ni Thin Films with Different Thicknesses on the Substrate Temperature

Farnaz Maghazeii *

Department of Mathematics and Physics, Science Faculty, Islamic Azad University Arak Branch, Arak, Iran

ARTICLE INFO

Article History:
Received 22 June 2017
Accepted 12 August 2017
Published 01 October 2017

Keywords:
Film Thickness
Kramers-Kronig
Ni Thin Films
Optical Properties
Substrate Temperature
Void Fractions

ABSTRACT

Nickel films with the thicknesses of 30 and 120 nm were deposited on glass substrates, at different substrate temperatures (313 to 600 K) under uhv condition. The nano-structure of the films and mean diameter of grains was obtained for each films using atomic force microscopy (AFM). Their optical properties were measured by spectrophotometry in the spectral range of 190-2500 nm. Kramers-Kronig method was used for the analysis of the reflectivity curves. The Effective Medium Approximation (EMA) analysis was used to determine the values of volume fraction of voids (f_v) and establish the relationship between the nanostructure of the film and EMA predictions. Qualitatively good agreements between structure Zone Model (SZM) as a function of substrate temperature and the values of (f_v), is achieved. There is good agreement between these values and the results of mean diameter of grains for Ni films too. The absorption peaks of Ni thin films at ~ 1.4 eV and 5 eV are observed, with an additional bump at about 2 eV. The 1.4 eV peak is in particular much stronger than that obtained in earlier works on Ni thin films and on bulk Ni sample. This is resulted from producing thin films under uhv condition. The conductivities σ_1 and σ_2 calculated from ε_1 and ε_2 for Ni films and were plotted vs energy.

How to cite this article
Maghazeii F. Dependence of Nanostructure and the Optical Properties of Ni Thin Films with Different Thicknesses on the Substrate Temperature. J Nanostruct, 2017; 7(4):273-283.

INTRODUCTION

Nickel is a ferromagnetic material that has found wide application in the form of thin films and that is essential for modern technologies [1]. Fabrication of nanostructured nickel thin films is of importance due to its potential applications is diverse fields such as high density recording media, ferrofluid technology, spin valves, magnetic resonance imaging, magnetocaloric refrigeration and as catalyst for the growth of carbon nanotube [2-5].

Extensive studies of the correlation between film nanostructure and deposition parameters have been carried out over the past five decades. From an understanding of film formation,follows the possibility for microstructural engineering in order to design a material for specific technological applications [6]. This has led to the development and refinement of Structure Zone Model (SZM).In this model the influence of substrate temperature on the structure of metallic thin films has been reported by Movchan and Demchishin for evaporated and by Thronton [7] for sputtered thin films for the broad description of polycrystalline film structure, which consists of three zones, separated by two boundary temperatures at

* *Corresponding Author Email: f_maghazeii@iau-arak.ac.ir*

Ts ~ 0.3Tm and Ts ~ 0.45Tm (Ts and Tm are the substrate and the material's melting temperatures in kelvin, respectively). In general, zone I consists of porous structure (tapered crystallites separated by voids), zone II, consists of columnar grains with smooth surfaces and in zone III the grain structure re-crystallizes.

It is well known that grain size in thin metallic films increase with the substrate temperature [8-10]. Hence, the grain boundaries change, due to diffusion processes. Both the mobility and the activation energy for the migration of a grain boundary depend on its crystallography [11]. Accordingly, at any given temperature, boundaries with different crystallography will migrate at different rates and the lower the temperature the smaller the proportion of mobile boundary types. Therefore, it is of interest to find out the relationship between Thin films' optical parameters and the structural changes described by variations of substrate temperature (SZM) [7,11-14].

MATERIALS AND METHODS

Nickel (99.99+% purity) films with the thicknesses of 30 and 120 nm were produced by electron beam evaporation using a Balzers UMS 500U UHV plant, on float glass substrates of rms surface roughness R_q of 0.35 nm, at four different substrate temperatures 313, 400, 500 and 600 K. A nominal deposition rate of 1.0 $Å s^{-1}$ was used. The nominal film thickness was measured after deposition using a Rank Taylor Hobson Talystep profilometer. A base pressure of ~ 5 x 10^{-9} mbar was achieved and the residual gas was composed mainly of H_2, H_2O, CO and CO_2, as detected by the quadrupole mass spectrometer. The deposition rate was monitored by a quadrupole mass spectrometer and controlled by feedback to the evaporation source. In all cases, the substrate normal was at 8.5º to the direction of incidence of the evaporant beam and the distance between the evaporation crucible and substrate was 54.5 cm. The deposition process was repeated several times and the reproducibility of the optical results (i.e., optical reflection from similar films produced) was confirmed.

Just before use all glass substrates were ultrasonically cleaned in heated acetone then ethanol. The near normal incidence reflectance spectra are obtained using a double beam spectrophotometer (Carry 500) in the spectral range of (190-2500 nm) corresponding to the energy range of (0.5-6.5 eV).

The film surface morphology and roughness was obtained by means of atomic force microscopy (AFM) (Park Scientific).

For determining of optical constants of Ni films, we used Kramers-Kronig relations. Void fraction contents (f_v) for each film obtained with the help of the Effective-Media Approximation (EMA) analysis.

It should be emphasized here that each film was produced at a set substrate temperature in the UHV system and after the process of deposition was completed it was let to cool down to room temperature in vacuum and the optical measurements were carried out at room temperature. This is different from the previously reported limited works on bulk [15-18] or thin film [19] in which the annealing procedure or heating the sample during optical measurements was employed. It is also worthwhile to emphasize that the annealing procedure totally changes the film structure from its original shape, while the heating the sample during optical measurements changes the structure continuously and hence the electronic structure. On the other hand, when measurements are carried out at room temperature on films produced at different substrate temperatures under uhv condition, no structural changes are expected to occur. Finally it should also be pointed out that for example in most optical and magnetic applications of metallic thin films, films "as deposited" are favored, for annealing causes crystallization and may deform the substrate.

RESULTS AND DISCUSSION

surface morphologies obtained by AFM

Fig. 1 shows the 3D AFM images of 30 and 120 nm Ni films produced at different substrate temperature respectively. The RMS roughness obtained for each film is also included under each 3D AFM image.

The results in Fig. 1 show the diffusion effect which causes larger grains to grow with increasing the substrate temperature clearly. Grow of grains is very more obvious for thicker films, whereas in the same temperatures, the size of grains in the thicker films is larger than of thinner films.

Hillocks observed for films produced at lower substrate temperatures are stress induced protrusions of material common to metal thin films

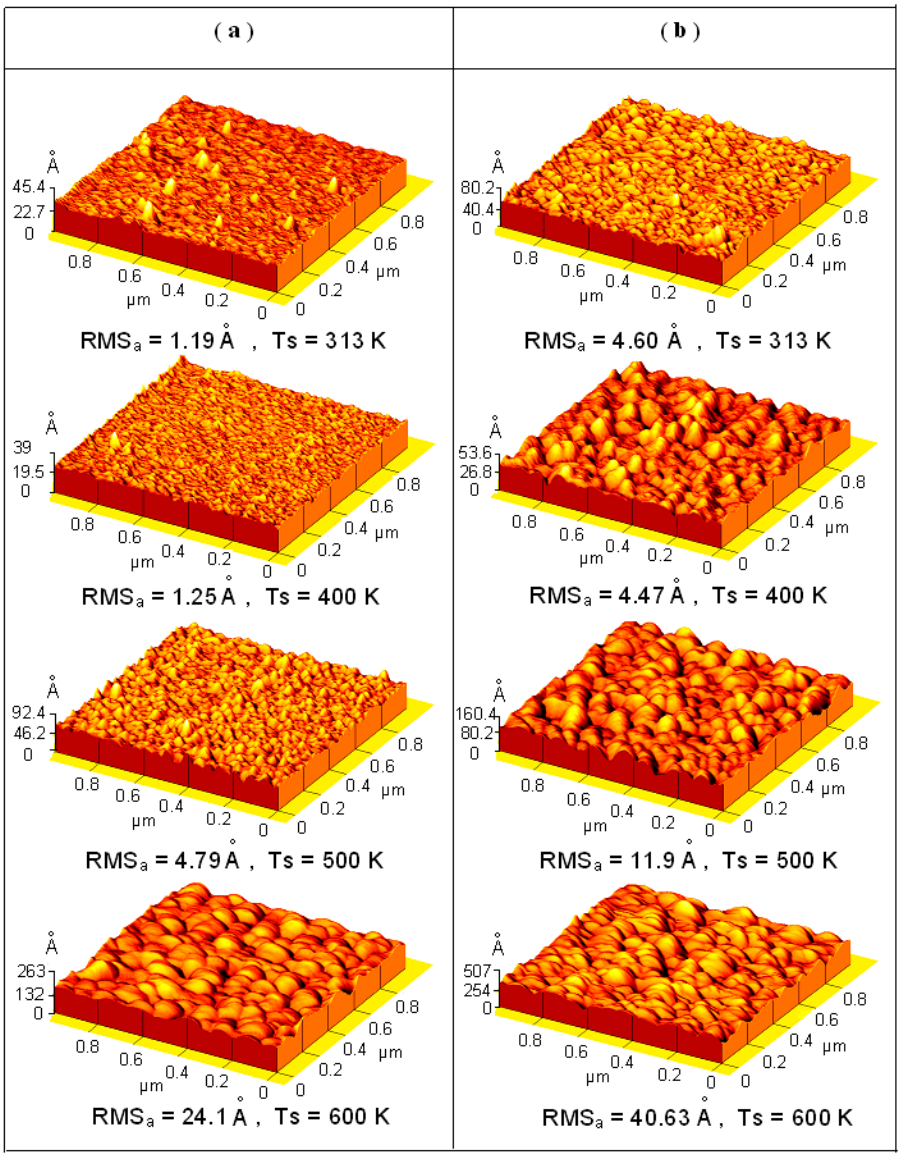

Fig. 1. 3D AFM images of: a) 30 nm & b) 120 nm Ni/glass films produced at different substrate temperatures.

deposited with compressive film stress as a stress relief mechanism. As the substrate temperature increases, hillocks disappear, hence the tensile stress should develop in these films.

The results of surface roughness measurement showed that the surface roughness increases with substrate temperature. Again this increase is expected as films' surface structure, as seen in 3D AFM images too, changes from almost smooth with some hillocks to grains with valleys between them.

Fig. 2 and Fig. 3 show the 2D AFM images of 30 and 120 nm Ni films with different substrate temperatures. From these images, the mean diameter for grains is measured For all of the films.

Table 1 shows these measures in terms of different temperatures for two different thicknesses. As we can see, the size of grains increase with temperature and this increase is more regular for thicker films. The presence of hillocks arising from stress in thinner films is the reason of this problem.

Grow of the grains causes the decrease of holes and void fractions and consequently, the density of the films is increased.

Optical constants of Ni films

Kramers-Kronig relations were used according to the method described in detail in [20] to convert

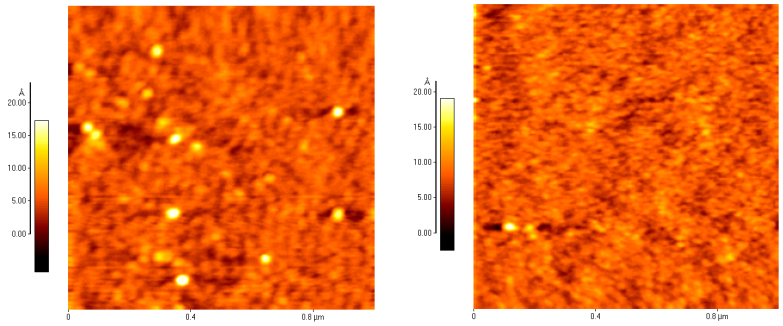

d = 30 nm , Ts = 313 K **d = 30 nm , Ts = 400 K**

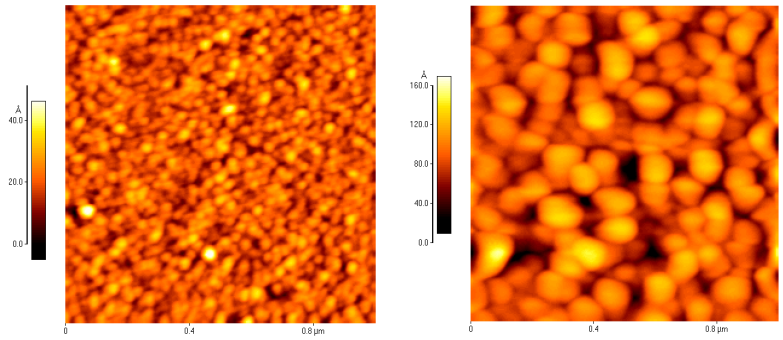

d = 30 nm , Ts = 500 K **d = 30 nm , Ts = 600 K**

Fig. 2. 2D AFM images of 30 nm Ni/glass films produced at different substrate temperatures.

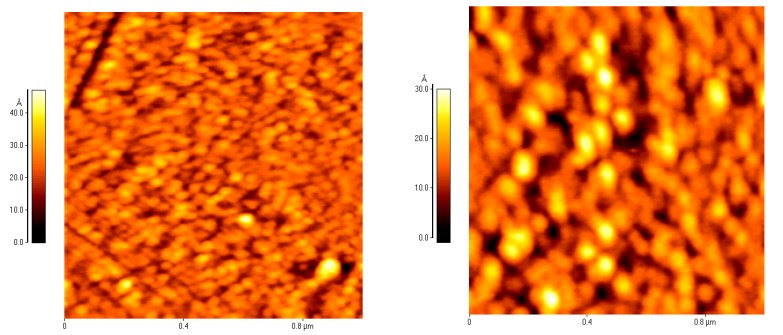

d = 120 nm , Ts = 313 K **d = 120 nm , Ts = 400 K**

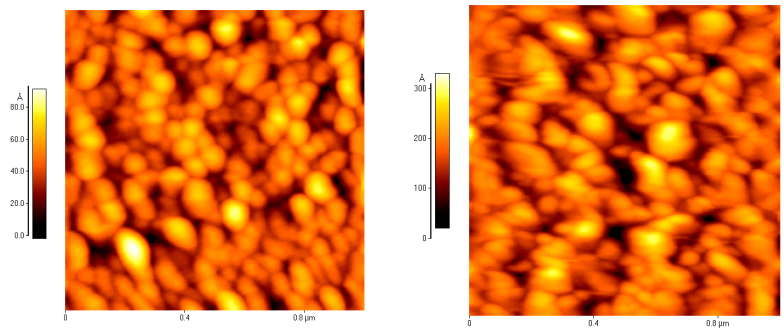

d = 120 nm , Ts = 500 K **d = 120 nm , Ts = 600 K**

Fig. 3. 2D AFM images of 120 nm Ni/glass films produced at different substrate temperatures.

Table 1. The mean values of grain diameters according to (nm) for the films with 30 and 120 nm thicknesses in different substrate temperatures.

Substrate temperature (K) / Film thickness (nm)	313	400	500	600
30	34.8	25.1	36.1	92.4
120	43.3	68.1	76.1	154.2

the measured reflectivity spectra to spectra of the complex dielectric function, from which the optical conductivity and other parameters were calculated.

Fig. 4 and Fig. 5 show the spectra of ε_1 and ε_2 for Ni/glass films of 30 nm (part a) and 120 nm (part b) produced at four different substrate temperatures (i.e., 313, 400, 500 and 600 K). Johnson and Christy's results [22] for thin Ni films ranging between 28 to 40 nm and Lynch et al's results [18] for single crystal at 4 K up to 3.0 eV and Ehrenrich et al [20] for bulk electrolytically etched Ni samples are also included for comparison. The Ehrenrich et al's data is presented in Fig. 2 of reference [20] from ~ 2.0 eV up wards. In the overlap region of 2.0 eV to 3.0 eV between Lynch et al's data and Ehrenrich et al's data there is a good agreement and the average of the two sets were accepted for the presentation in all figures in this work. Hereafter this result will be called "bulk sample [18,20]". The general trend of our results is similar to those of Johnson and Christy [22] and of bulk sample [18,20].

Both ε_1 and ε_2 show temperature dependence. The ε_1 and ε_2 in Fig. 4 and Fig. 5 show that the values obtained above ~ 3.0 eV, in particular for lower substrate temperatures are almost similar and are closer to both Johnson and Christy's and bulk sample's [18,20] results (except for (120nm, 600 K) film). The major deviations occur at energies below 3.0 eV, and particularly at less than 2.0 eV, where a peak at about 1.4 eV can be observed with different strengths in ε_1 Fig. 4 at different substrate temperatures and thicknesses . Shiga and Pells [21] have assigned this peak to the transition between the bands near the W and K symmetry points. At some energy regions curves cross each other hence suggesting energy dependence too. The peak at ~ 1.4 eV can be observed for all films with different strengths, though in some cases it looks only as a bump. The variation of the strength of this peak as a function of substrate temperature for both thicknesses is given in Fig. 6. In Fig. 6 it can be observed that the strength of this peak decreases with increasing the

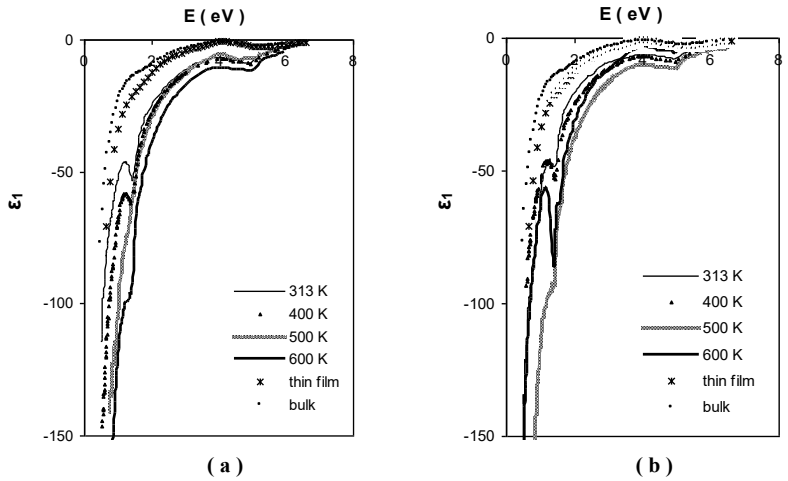

Fig. 4. The real part of the dielectric constant of : a) 30 nm & b) 120 nm Ni / glass films produced at different substrate temperatures. thin film) Thin Film sample; bulk) Bulk sample.

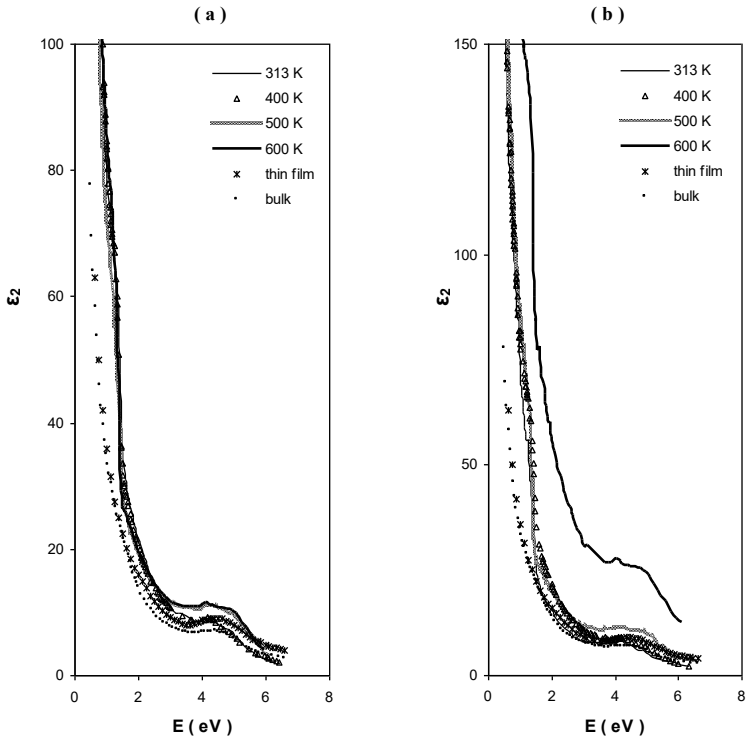

Fig. 5. The imaginary part of the dielectric constant of : a) 30 nm & b) 120 nm Ni / glass films produced at different substrate temperatures. thin film) Thin Film sample; bulk) Bulk sample.

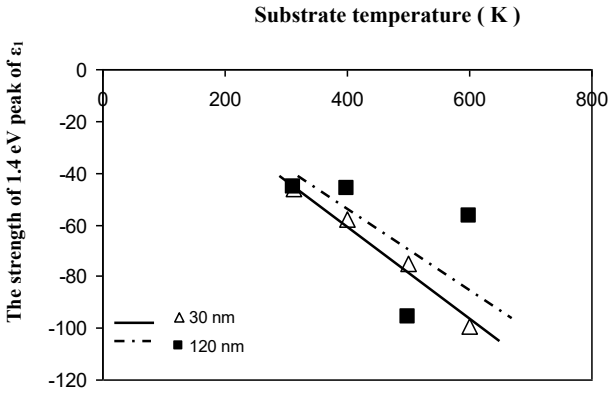

Fig. 6. The strength of 1.4 eV peak in the real part of the dielectric function of 30 and 120 nm Ni/glass films as a function of substrate temperature.

substrate temperature, which can be the result of increased diffusion process due to increase of substrate temperature; confirmed in Section 3.1 by AFM images.

Shiga and Pells [18] reported that an unclean surface gives a weaker peak/bump. In addition Savaloni et al [9, 10], used a quadrupole mass spectrometer and analyzed the partial pressure of the residual gas inside their uhv chamber (the same system used in this work) before and after deposition of erbium at different base pressures as a function of substrate temperature. They reported that the substrate holder assembly is an important site for out gassing and for reactions, including those between deposited erbium and residual gases. In particular they found that water decomposes at about 600 K (see Fig. 4 in ref. [10]). They suggested that the water and its

products arise from out gassing and reactions at the substrate and substrate holder. Therefore, it may be concluded that the higher intensity of 1.4 eV peak in our work is due to the lower amount (partial pressure) of oxygen, hence it was probable that less thick oxide layer was formed.

Apart from the peak at ~ 1.4 eV in ε_1 spectra, the other distinguishable feature is the minimum at about 5 eV, which is also observed and reported by Johnson and Christy [19] and bulk sample [15,17].

The mechanisms involved in the temperature dependence of ε_2 in metals are summarized by Rosei and Lynch [21] as; volume thermal expansion (shear strains resulting from different thermal-expansion rates in the substrate and sample), increased phonon population, Fermi-distribution broadening, and shift of Fermi level. These thermal mechanisms cause small energy shifts in band structure or Fermi level of the metals. As a result, these shifts give small shifts in the position of peaks in the ε_2 vs. photon energy curve, which are seen as changes in the magnitude of ε_2 at a given energy. The latter shift and the change of magnitude in ε_2 vs. photon energy is distinguished over the whole energy range in this work. The former shift regarding energy shift in band structure, because of the shape of the ε_2 curves in Fig. 5 can only be discussed qualitatively and in general terms as follows: If the position of the peak (bump) between 3.5 and 5.5 eV is considered for this reason it can be noticed that this shift is not present neither with variation of substrate temperature nor with increasing the film thickness.

The other feature which may influence the optical results is the presence of an over-layer (oxide layer) on the film. The over layer thickness for all of the films calculated in previous research [22] and a value of less than 2 nm obtained. On the other hand, in none of the results of ε_2 for Ni films a shift in peak energy can be seen, therefore these over-layers (if at all present) is negligible and have no significant effect on the results, while the shift in the height of the ε_2 spectra is an indication of the influence of the film surface roughness and morphology.

Absorption coefficients and conductivities for Ni films

Experimental absorption coefficients,$\alpha(E)= (2E/hc)\ K(E)$, obtained for Ni films of 30 and 120 nm thicknesses produced at different substrate temperatures are plotted in Fig. 7 along with the results of Johnson and Christy [19] (for thin film) and bulk sample [15,17]. In Fig. 7 it can be observed that the general trend of the variation of the results for Ni films is similar to those of Johnson and Christy [19], and bulk sample [15,17]. In Fig. 7 it can be distinguished that the absorption increases with substrate temperature and this increment is more evident for (30 nm, 600 K) whereas in the thicker films (120 nm thickness), prominent increase of absorption is started from the lower temperature (500 K). This is due to increased diffusion, and change of surface topography from amorphous/fibrous structure (more specular surface topography) to columnar/

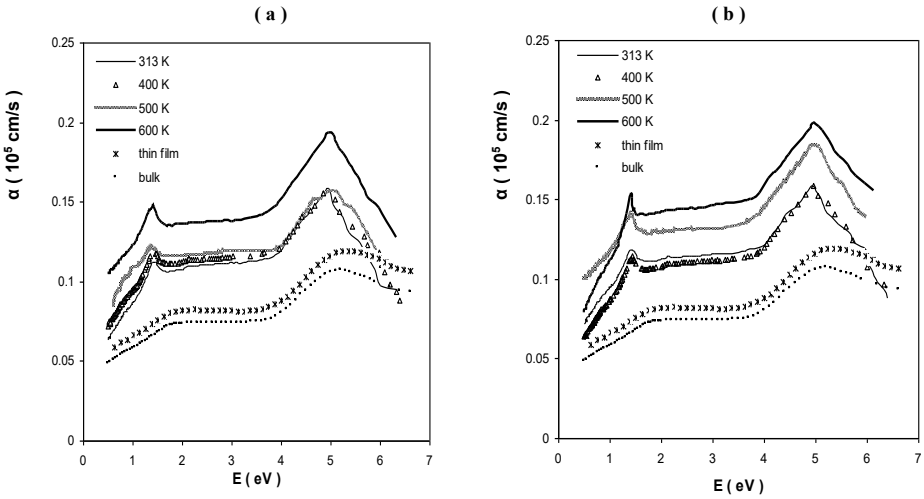

Fig. 7. Absorption coefficient vs. energy for : a) 30 nm & b) 120 nm Ni/glass films produced at different substrate temperatures. thin film) Thin Film sample; bulk) Bulk sample.

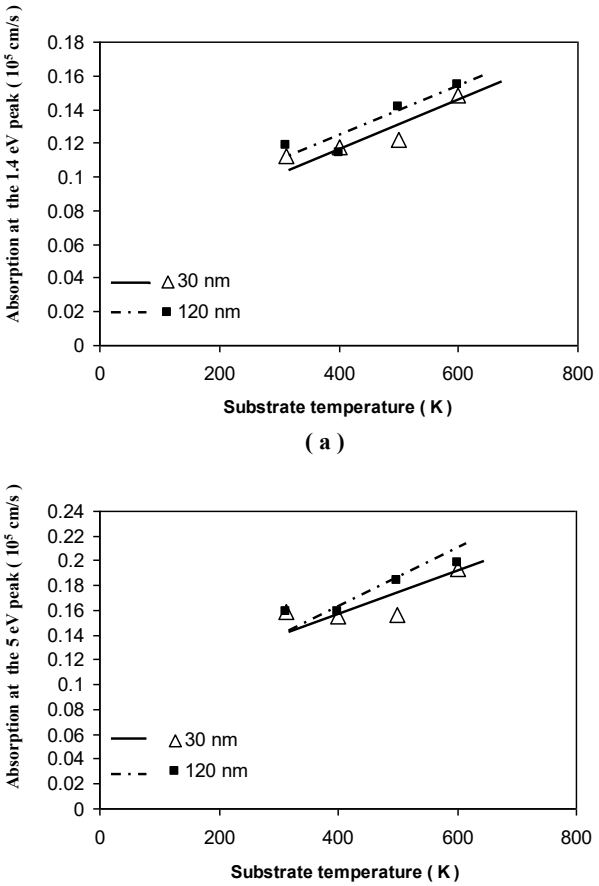

Fig. 8. a) The strength of 1.4 eV (minor) peak in the absorption coefficient of 30 and 120 nm Ni/glass films as a function of substrate temperature. b) The strength of 5.0 eV (main) peak in the absorption coefficient of 30 and 120 nm Ni/glass films as a function of substrate temperature

grain structure, hence increased surface roughness due to possible grooving-like effect/deep valleys as well as increased amount of oxide as discussed in section 3.2.

The film with 30 nm thickness which produced at lowest substrate temperature (i.e., 313 K) show closer agreement to that of Johnson and Christy's results (i.e., 28-40 nm thin Ni films). In general, in the structure reported for the absorption of nickel, two peaks at ~ 1.4 eV (small peak) and ~ 5.0 eV (large principal peak) are reported [15-17,23].

In Fig. 7 two clear peaks at ~ 1.4 eV and ~ 5.0 eV can be observed with different strengths, while they are stronger than those in Johnson and Christy's results [19] and bulk sample's results [15,17]. In particular the smaller peak at ~ 1.4 eV is more pronounced in our results. This might be due to the production procedure of our films which were deposited under uhv (10^{-9} mbar) condition from 99.99+% pure nickel source.

The variation of the strength of both absorption peaks (i.e., the peak at ~ 1.4 eV and the peak at ~ 5.0 eV) as a function of substrate temperature for both thicknesses is given in Fig. 8. The variation of the strength of both peaks with substrate temperature is the same and increase linearly with substrate temperature.

Interband region for Ni films in details was studied in ref. [22].

In case of transition metals it is usually more convenient to plot conductivity $\sigma_1 + \sigma_2$ rather than ε_1 and ε_2 , since ε_2 becomes infinite at zero frequency, whereas σ remains finite, any structure in the optical constants at low frequencies will be much more evident in the conductivity. σ_1 and σ_2 are given as [19]:

$$\sigma_1 = \frac{\varepsilon_2 \omega}{4\pi} \quad (1)$$

$$\sigma_2 = \frac{(1-\varepsilon_1)\omega}{4\pi} \quad (2)$$

The conductivities σ_1 and σ_2 calculated from ε_1 and ε_2 for Ni films are plotted in Figs. 9 and 10, respectively. It can be observed that again the trends of variation of both σ_1 and σ_2 results for Ni films are similar to both Johnson and Christy's and bulk sample's results. However, the absolute values obtained in this work for σ_1 and σ_2 are greater than those of Johnson and Christy [19] and bulk sample [15,17]. In Fig. 9, again two peaks at ~ 1.4 eV and ~ 5.0 eV are vividly present and also it can be observed that the real part of conductivity, in general, increases with substrate temperature. These results are expected as a consequence of the increase in diffusion effects due to increased substrate temperature (larger grains formed, hence less grain boundaries are present) [6].

Effective-media approximation (EMA) approach

The correlation between nickel thin film nano-structure and its optical property as a function of substrate temperature has been one of the aims

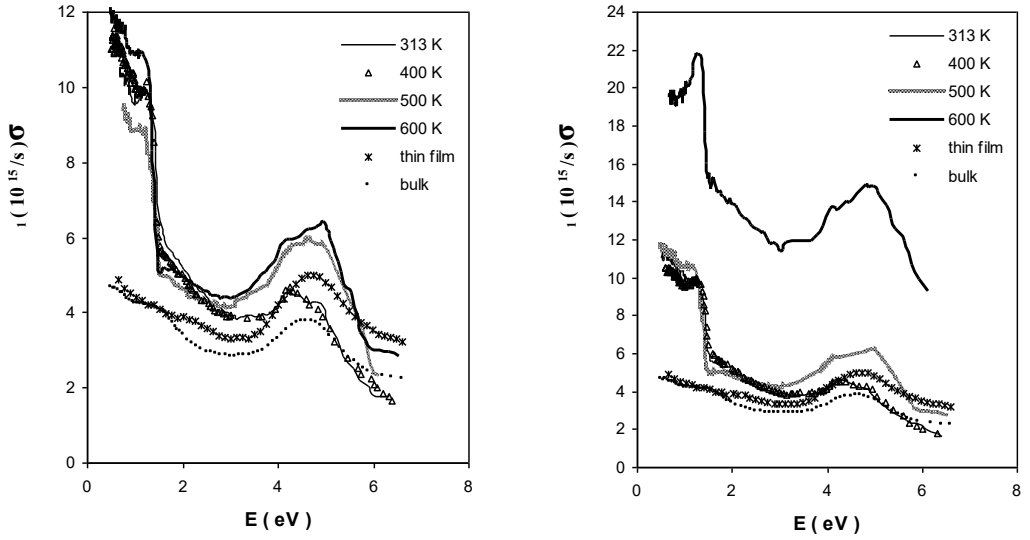

Fig. 9. The real part of the optical conductivity vs. energy for : a) 30 nm & b) 120 nm Ni/glass films produced at different substrate temperatures. thin film) Thin Film sample; bulk) Bulk sample.

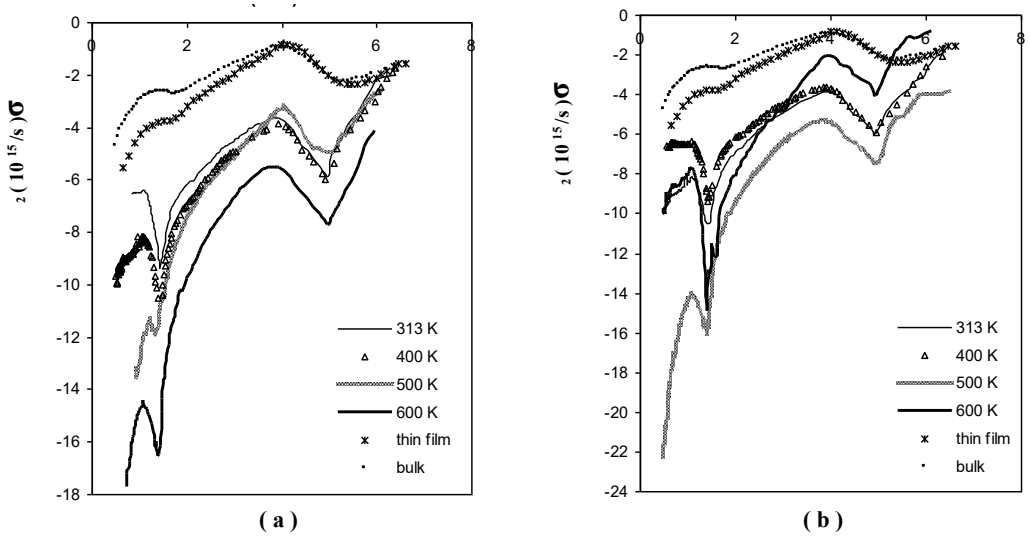

Fig. 10. The imaginary part of the optical conductivity vs. energy for : a) 30 nm & b) 120 nm Ni/glass films produced at different substrate temperatures. thin film) Thin Film sample; bulk) Bulk sample.

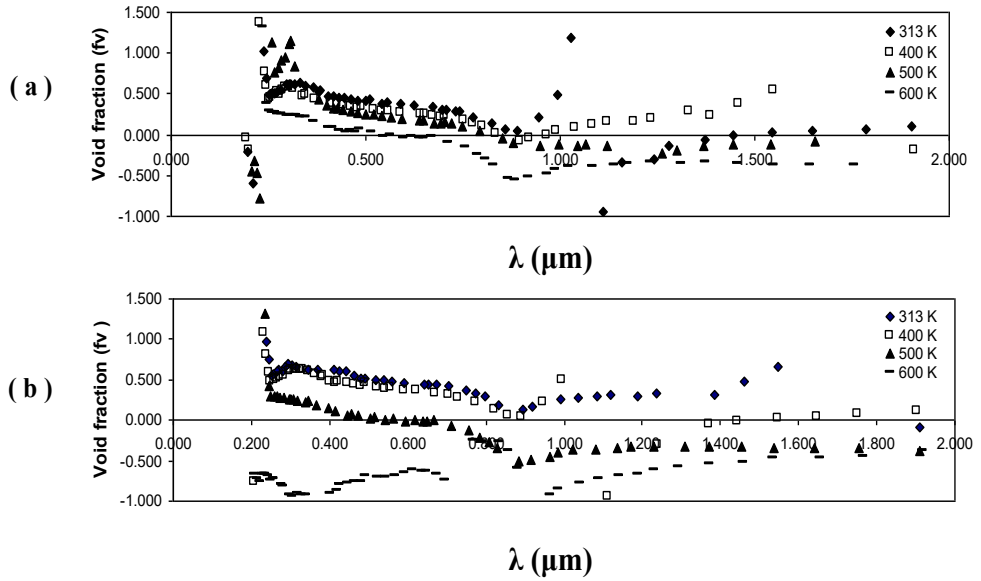

Fig. 11. Void fraction vs. wavelength for : a) 30 nm and b) 120 nm Ni/glass films produced at different substrate temperatures.

of this work, which can be achieved through using the effective-media approximation (EMA).

The effect of voids on the optical properties of thin films may be investigated by the effective-media approximation [24,25]:

$$\frac{\langle\varepsilon\rangle-\varepsilon_h}{\langle\varepsilon\rangle+2\varepsilon_h}=f_v\frac{1-\varepsilon_h}{1+2\varepsilon_h}+(1-f_v)\frac{\varepsilon-\varepsilon_h}{\varepsilon+2\varepsilon_h}, \quad (3)$$

where, , <ε> is the effective dielectric function of heterogeneous material containing a volume fraction, f_v of voids and ε_h is the dielectric function of the host material.

In equation (1) if we take $\varepsilon_h = \langle\varepsilon\rangle$ the Bruggeman (EMA) can be obtained, which treats both void and material phases on equal, self-consistent basis. We have:

$$f_v\left[\frac{1-\varepsilon_h}{1+2\varepsilon_h}\right]=(f_v-1)\left[\frac{\varepsilon-\varepsilon_h}{\varepsilon+2\varepsilon_h}\right]. \quad (4)$$

Using equation (2) in which ε are the values for bulk metal [15], the fraction of voids for Ni films was obtained by least square fit to equation (2). The least square fit procedure to equation (2) was carried out by minimization of the real and the imaginary parts of equation (2) separately, while f_v was the adjusting (search parameter). The value of f_v which minimized both real and imaginary parts of equation (2) was accepted for void fraction.

The results of f_v for Ni/glass films of 30 and 120 nm thicknesses produced at four different substrate temperatures are given in Fig. 11a and Fig. 11b respectively. In these figures, $f_v=0$ line represents the void fraction value for bulk (reference) material, and positive and negative values of f_v represent films with lower and higher densities than for bulk, respectively, as explained by Aspnes [25].

The variation of the void fraction with substrate temperature shows that the density increases with substrate temperature. This is in agreement with the predictions of the structure zone model presented in section 1 and the results of mean diameter of grains for films mentioned in section 3.1 ; as the substrate temperature increases, owing to the enhanced diffusion effects, the grain size and the film density increase, while the fraction of voids in the film decreases.These results have good agreement with the values of f_v for Ag and Cu in ref.[20].

In general, so far as the substrate temperature is concerned one can conclude that the results of void fraction are qualitatively in agreement with the structure zone model.

CONCLUSIONS

The relationship between the nanostructure of Ni thin films produced under different uhv conditions and their optical properties is accomplished by studying the relationship between SZM and EMA, while the EMA results in turn are

dependent on the dielectric constant of both film and bulk samples. The optical constants of these films showed that the dispersion behaviors are sensitive to the deposition condition. Defects such as voids in the structure as well as the different phenomena/activated processes involved in the film evolution could be responsible for these observations. The results for different substrate temperatures showed that the fraction of voids obtained, using EMA method qualitatively agree well with the predictions of SZM model. There is good agreement between f_v contents and the results of mean diameter of grains for Ni films too. The 1.4 eV and 5.0 eV absorption peaks of Ni thin films are observed . The higher strength of peaks in different sets of data in our work can be related to the higher purity of our films produced under uhv condition.

ACKNOWLEDGEMENTS

This work was carried out with the support of the University of Tehran, and Islamic Azad University. We also thank from dear Mr. Jafari.

CONFLICT OF INTEREST

The authors declare that there are no conflicts of interest regarding the publication of this manuscript.

REFERENCES

1. Potocnik J, Nenadovic M, Jokic B, Strbac S, Rakoeevic Z. Structural characterization of the Nickel thin film deposited by GLAD technique. Science of Sintering. 2013; 45: 61-67.
2. Kumar P. Magnetic behavior of surface nanostructured 50 nm Nickel thin films. Nano scale Res. Letters. 2010; 5: 1596-1602.
3. Song W K, Jing L, Podraza N J, Dickey E C. Spin spray-deposited Nickel manganite thermistor films for microbolometer applications. J. of the American Ceramic Society. 2011; 11: 516-523.
4. Otiti T, Ekosse G, Sathiaraj, Stephen T. Understanding Nickel Thin Film crystallization using X-Ray Diffractometry. J. Appl. Sci. Environ. Manage.. 2007; 11: 57-60.
5. Luo J K, Flewitt A J, Spearing S M, Fleck N A, Milne W I. Young's modulus of electroplated Ni thin film for MEMS applications. Materials Letters. 2004; 58: 2306-2309.
6. Petrov I, Barna P B, Hultman L, Greene J E. Microstructural evolution during film growth. J. Vac. Sci. Technol.. 2003; A 21: S117-S128.
7. Thoronton J A. Structure and topography of sputtered coatings. J. Vac. Sci. Technol.. 1975; 12: 830-838.
8. Savaloni H, Bagheri-Najmi S. Characteristics of Cu and Zn films deposited on glass and stainless steel substrates at different substrate temperatures and angle of incidence. Vacuum. 2002; 66: 49-58.
9. Savaloni H, Player M A. Influence of deposition conditions and kind of substrate on the structure of uhv deposited Erbium films. Vacuum. 1995; 46: 167-179.
10. Savaloni H, Player M A, Gu E, Marr G V. Influence of substrate temperature,deposition rate, surface texture and material on the structure of uhv deposited Erbium films. Vacuum. 1992; 43: 965-980.
11. Grovenor C R M, Hentzell H T G, Smith D A. The development of grain structure during growth of metallic films. Acta Metall. 1984; 32: 773-781.
12. Hentzell H T G, Grovenor C R M, Smith D A. Grain structure variation with temperature for evaporated metal films. J. Vac. Sci. Technol.. 1984; A2: 218-219.
13. Messier R, Giri A P, Roy R A. Revised structure zone model for thin-film physical structure. J. Vac. Sci. Technol.. 1984; A2: 500-503.
14. Messier R. Toward quantification of thin film morphology. J. Vac. Sci. Technol.. 1986; A4: 490-495.
15. Lynch D W, Rosei R, Weaver J H. Infrared and visible optical properties of single crystal Ni at 4K. Solid State Commun.. 1971; 9: 2195-2199.
16. Roberts S. Optical properties of Nickel and Tungsten and their interpretation according to Drude's formula. Phys. Rev.. 1959; 114,: 104-115.
17. Ehrenreich H, Philipp H R, Olechna D J. Optical properties and Fermi surface of Nickel. Phys. Rev.. 1963; 131: 2469-2477.
18. Shiga M, Pells G P. The optical properties of Nickel above and below the Curie temperature. J. Phys. C (Solid St. Phys.). 1969; 2: 1847-1857.
19. Johnson R B, Christy R W. Optical constants of transition metals: Ti,V,Cr,Mn,Fe,Co,Ni and Pd. Physical Review. 1974; B9: 5056-5070.
20. Savaloni H, Khakpour A R. Substrate temperature dependence on the optical properties of Cu and Ag thin films. Eur. Phys. J. Appl. Phys. 2005; 31: 101-112.
21. Rosei R, Lynch D W. Thermomodulation spectra of Al,Au and Cu. Phys. Rev.. 1972; B5 : 3883-3894.
22. Maghazeii F, Savaloni H, Gholipour-Shahraki M. The influence of growth parameters on the optical properties and morphology of uhv deposited Ni thin films. Optics Commun. 2008; 281: 4687-4695.
23. Stoll M Ph. Optical properties of Nickel in the visible and near infra-red. Solid State Commun.. 1970; 8: 1207-1210.
24. Bruggemann D A G. Calculation of different physical constants of heterogeneous substances, dielectric constants and conductivities of the mixed bodies of isotropic substances. Ann. Phys. (Leipzig). 1935; 24: 636-664.
25. Aspnes E, Kinsbron E, Bacon D D. Optical properties of Au: sample effects. Phys. Rev.. 1980; B21: 3290-3298.